3 Iron nitrides

3.1 Introduction

Over the past decades the interest in the iron−nitrogen system was triggered both from a fundamental and a technological point of view. Among the applications, iron nitrides have found significant interest as materials for magnetic storage devices or in the coating industry. The first phase diagram of iron nitrides was delivered by Jack [22] as early as 1951. Since then, additional efforts were aimed at further understanding the physics and the chemistry of these compounds, reveal their properties or synthesize new phases.

A more recent phase diagram (see Fig. 3.1) extended to low temperatures was proposed by du Marchie *et al.* [23]. Most of the phases in this phase diagram were experimentally confirmed, being synthesized as pure phases or in mixtures of phases. Depending on the nitrogen content, iron nitride phases with different structure and properties can be formed. All iron nitrides are metallic conductors and metastable with respect to decomposition into Fe and N_2. The decomposition is limited by kinetic barriers. Atomic nitrogen can be dissolved in the body−centered cubic (bcc) lattice of $\alpha-$Fe to a concentration of about 0.4 at.% N without much distortion of the lattice. Higher concentrations of nitrogen can be introduced by quenching γ austenite Fe (which can dissolve up to 10.3 at.% N). Alternative methods are sputtering Fe in the presence of nitrogen, or by $\alpha-$nitriding Fe containing a few at.% of an alloying metal that forms nitride precipitates, thereby dilating the Fe lattice [24].

When more than 2.4 at.% N is dissolved in pure Fe, the bcc lattice undergoes a tetragonal deformation. In the composition range up to about 11 at.% N, the iron nitride compound is called nitrogen martensite α'. This phase has a body centred tetragonal (bct) structure with lattice parameters depending on the nitrogen content. The N atoms occupy randomly octahedral hollow sites in the Fe sublattice. At saturation, nitrogen martensite has the Fe_8N composition. The $\alpha'-Fe_8N$ can transform into the $\alpha''-Fe_{16}N_2$ phase. In this phase, the N atoms are ordered. It can be formed under special conditions from Fe, however, not in its pure form. The $\alpha''-Fe_{16}N_2$ phase attracted considerable attention because of a possible very high saturation magnetization, reported to vary between 2.4 T and 3.2 T. Such a value would be the highest

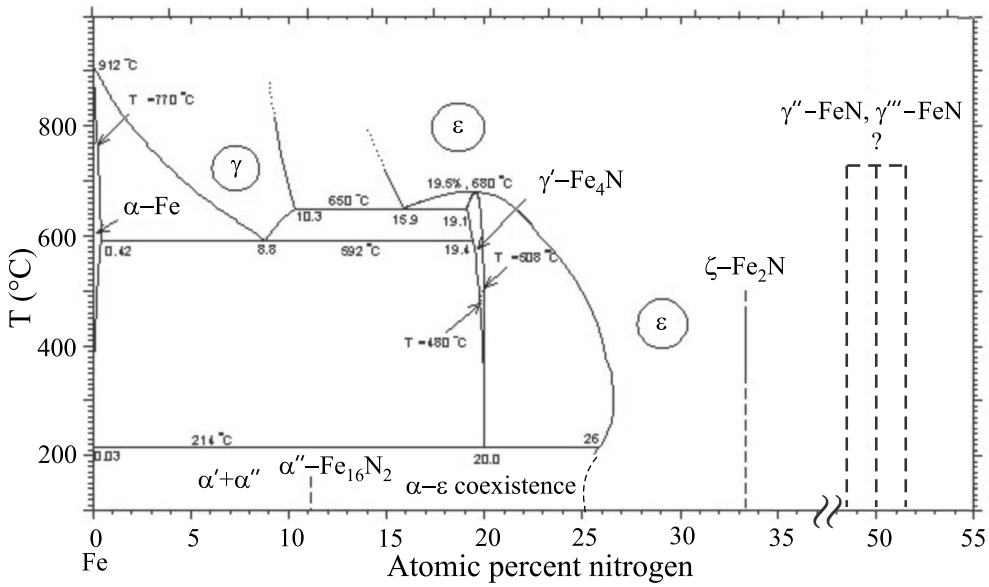

Figure 3.1: *The Fe−N phase diagram based on the one of du Marchie [23] and augmented with the $\gamma''-FeN$ and $\gamma'''-FeN$ phases.*

of all known materials. However, this item remains a controversy both from the theoretical and the experimental point of view, despite the huge amount of research. One of the crucial problems in getting a clear answer on the value of the saturation magnetization of the $\alpha''-Fe_{16}N_2$ phase is the lack of a pure, single crystalline phase.

The next phase in nitrogen content is the $\gamma'-Fe_4N$ phase (roaldite), which is cubic, with the Fe−sublattice arranged in a face centered cubic (fcc) structure and nitrogen atoms occupying the body−centered position one out of four. As indicated in the phase diagram (Fig. 3.1), this phase has a narrow composition range around 20 at.% N. The lattice parameter is 3.795 Å and the saturation magnetization was reported to be between 1.8 T and 1.9 T [25, 26, 27]. A saturation magnetization value in this range is slightly lower than the one of pure iron (2.21 T), making this phase somewhat less attractive in comparison with Fe. On the other hand, as a single crystalline material, the $\gamma'-Fe_4N$ phase has well defined magnetic properties [28] which makes it of interest in the growth of multilayers and structures for device applications [29, 30].

With increasing nitrogen content, the iron nitride phases change again structure. For a nitrogen composition ranging from 25 at.% N to 33 at.% N, the $\varepsilon-Fe_xN$ phase is formed, which has a hexagonal close−packed (hcp) structure. At the Fe_2N stoichiometry, the phase has an orthorhombic structure as a result of the ordering of the N atoms over the octahedral sites. This phase is called $\zeta-Fe_2N$. The $\varepsilon-Fe_xN$ phase is one of the most studied iron nitride phases, possibly due to the ease of growing it. Consequently, the change in

structural (lattice parameter) and magnetic properties as a function of nitrogen content was accurately determined leaving only few open questions. Increasing the nitrogen content in the ε phase, the unit cell expands, while the Curie temperature decreases drastically from 535 K (for the Fe_3N phase) to 9 K (for the Fe_2N phase). At room temperature, the change in Curie temperature corresponds to a gradual change in the magnetic character of the $\varepsilon-Fe_xN$ phase, from a ferromagnetic to a paramagnetic material [31].

Lately, it was brought forward [32, 33] that the phase diagram of iron nitrides can be extended further, to even more N−rich compounds, such as the $\gamma''-$FeN and the $\gamma'''-$FeN phases. The theoretical prediction of these two phases was made following the prediction and subsequent experimental confirmation of other MN compounds (M=metal, N−nitrogen). Based on theoretical calculations, as stoichiometric phases, both should have a nitrogen content of 50 at.% N but with a different configuration of the N atoms within the fcc Fe cage as shown in Fig. 3.2. The two structures correspond to the ZnS−type structure for the γ'' phase and a NaCl−type structure for the γ''' phase [34, 35, 36, 37, 38, 39, 40, 41]. The co−existence of a $\gamma''-$FeN and a $\gamma'''-$FeN phase is still a matter of controversy. As all the other iron nitrides, these two are also predicted to have a metallic character. Concerning their magnetic character, at room temperature both phases are reported to be paramagnetic, but the low temperature behavior is still under discussion.

According to Ching *et al.* [42], another iron nitride phase with even more nitrogen than the $\gamma''-$FeN and the $\gamma'''-$FeN, might exist. This phase, the Fe_3N_4, would have a spinel structure and a weakly ferromagnetic character. So far, there is no experimental evidence for the existence of this phase.

Due to the narrow nitrogen content borders, and the varying structural and magnetic properties with the formation of different phases, it is of crucial importance for many applications to produce single phase films. Over the years, this proved to be a rather challenging task together with an accurate

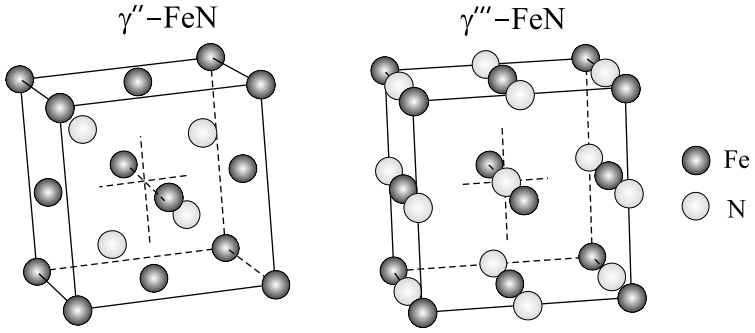

Figure 3.2: *Crystal structure of $\gamma''-$FeN and $\gamma'''-$FeN.*

phase identification. Till now, iron nitrides were mostly grown by sputtering, gas−assisted molecular beam epitaxy or gaseous nitriding of iron layers.

In this research, the growth of iron nitrides was probed in a different way, namely by molecular beam epitaxy of iron in the presence of atomic nitrogen as obtained from a rf atomic source. Additionally, the output of the atomic source was also used for post−nitriding freshly grown epitaxial Fe or iron nitride layers. One of the goals aimed at in this work was to get a perfect command of the growth of single phase iron nitride films and to determine the limiting parameters for the growth of a particular phase. The phase transformations taking place in the iron−nitrogen system were also investigated.

3.2 Experimental details

Iron nitride thin films were grown on clean and annealed (001) MgO substrates in an UHV system equipped with ^{57}Fe, natural Fe and Cu evaporators (Knudsen−cells). The films were grown using atomic nitrogen as obtained from a radio frequency (rf) atomic source. Two growth methods were applied: (a) molecular beam epitaxy (MBE) of iron in the presence of nitrogen obtained from the rf atomic source and (b) post−nitriding of freshly grown epitaxial iron layers or iron nitride layers with the output of the same rf atomic source.

Thin nitride films were produced by varying different growth parameters such as: deposition temperature, partial pressure of nitrogen or post−nitriding temperature. For phase identification, we explored the advantages of Conversion Electron Mössbauer spectroscopy (CEMS). The CEMS measurements were performed at room temperature or at 90 K (LT−CEMS). This method is quite accurate and enables an unambiguous distinction between different iron nitrides, iron oxides or additional iron-based phases. Also, it is sensitive to amounts which cannot be identified with other techniques (*e.g.* x−ray diffraction). The iron nitride films were also characterized with x−ray diffraction (XRD). The thickness of the films was measured by Rutherford backscattering spectrometry (RBS). All the films were grown with ^{57}Fe, yielding CEMS spectra with high statistics. To avoid oxidation in air, as−grown films could be capped in−situ with natural Fe or Cu.

3.3 $\alpha''-Fe_{16}N_2$

Up to now, despite the efforts, we were not able to synthesize $\alpha'-Fe_8N$ or $\alpha''-Fe_{16}N_2$ by MBE growth of iron in the presence of nitrogen from the rf atomic source. Therefore, another method was tried. The output of the source was used to nitride thin films of iron epitaxially grown on (001) MgO substrates. Different samples were grown by varying the mixture and the total pressure in the rf atomic source.

The highest fraction of $\alpha''-Fe_{16}N_2$ phase was obtained in a sample grown with the rf atomic source operating with pure N_2 at a pressure of 1×10^{-2} mbar. The output of the source was used to nitride a ∼42 nm thick iron layer at a temperature of 200°C. The nitriding time was 2 hours. After growth and cooling down to RT, the sample was measured ex−situ with CEMS and XRD. The corresponding CEMS spectrum is shown in Fig. 3.3. The major part of the spectrum was fitted with the components corresponding to $\alpha''-Fe_{16}N_2$ (three sextets; 22.1%), Fe (one sextet; 31.3%) and $\gamma'-Fe_4N$ (three sextets; 33.2%). The signature of each phase to the total CEMS spectrum is shown in Fig. 3.3 (a). The fit parameters for the $\alpha''-Fe_{16}N_2$ are given in Table. 3.1. The rest of the intensity (∼13%) in this spectrum is due to the oxide formed on top upon exposure to air. It is important to comment that the Mössbauer signature of $\alpha'-Fe_8N$ coincides with the one of $\alpha''-Fe_{16}N_2$. Therefore, CEMS cannot be used to distinguish the two phases and additional information from XRD measurements is needed.

An XRD scan measured for the same sample is shown in Fig. 3.4. While the peak at ∼58.8° corresponds to both the (002) reflection of $\alpha'-Fe_8N$ and the (004) reflection of $\alpha''-Fe_{16}N_2$, the reflection peak at ∼28.4° corresponds

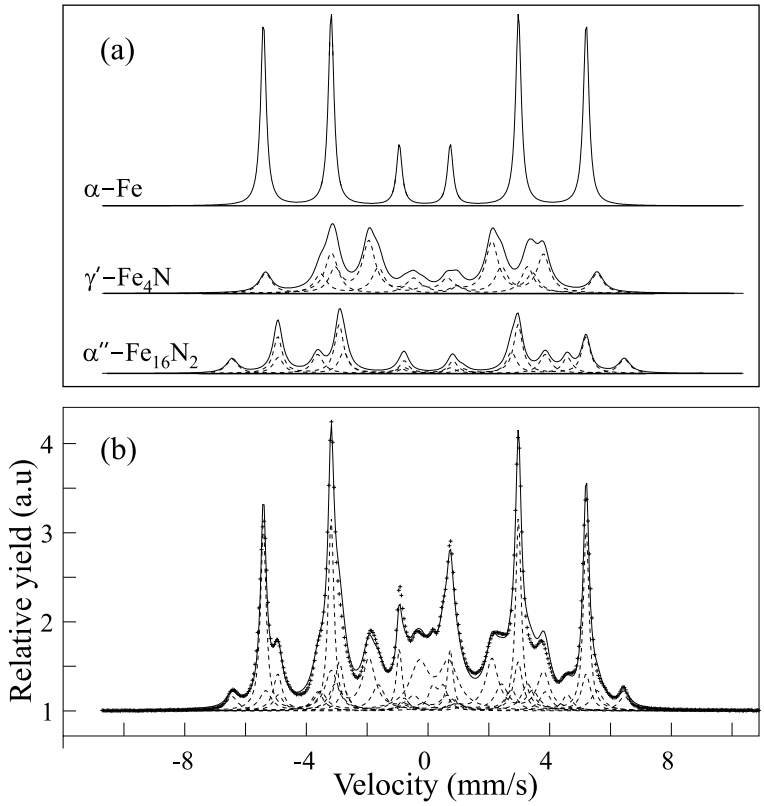

Figure 3.3: *Room temperature CEMS spectrum for a uncapped iron nitride film grown by post−nitriding of iron as a mixture of $\alpha''-Fe_{16}N_2$, Fe and $\gamma'-Fe_4N$.*

Table 3.1: *Mössbauer parameters of $\alpha''-Fe_{16}N_2$: δ−isomer shift (all given with respect to α−Fe at room temperature), H−hyperfine field, ε−quadrupole splitting, R.A−relative area.*

Component	δ (mm/s)	H(T)	ε (mm/s)	R.A.(%)
FeI	0.17	39.99	-0.1	25
FeII−A	0.17	31.42	0.1	50
FeII−B	0.01	29.46	-0.16	25

only to the (002) reflection of $\alpha''-Fe_{16}N_2$. This peak appears due to the ordering of the N atoms over the octahedral sites in the $\alpha''-Fe_{16}N_2$ phase and, consequently, a corresponding unit cell twice larger than the one of $\alpha'-Fe_8N$. The intensity ratio between the (004) and the (002) peaks of $\alpha''-Fe_{16}N_2$ was determined from x−ray scattering calculations [43] to be around 6.8. For our sample, the intensity ratio between the (004) and (002) reflections is close to this value, indicating the presence of $\alpha''-Fe_{16}N_2$, and no $\alpha'-Fe_8N$. The fact that we see XRD lines belonging to the $\alpha''-Fe_{16}N_2$ phase implies that small crystallites of the pure material must have been formed. Additional texture measurements showed that the $\alpha''-Fe_{16}N_2$ and Fe phases are epitaxial, with a 45° in−plane rotation with respect to MgO. The $\gamma'-Fe_4N$ phase was found to be almost epitaxial, with the (001) planes slightly tilted with respect to the sample surface. The tilt of ∼7° suggests that this phase is formed from

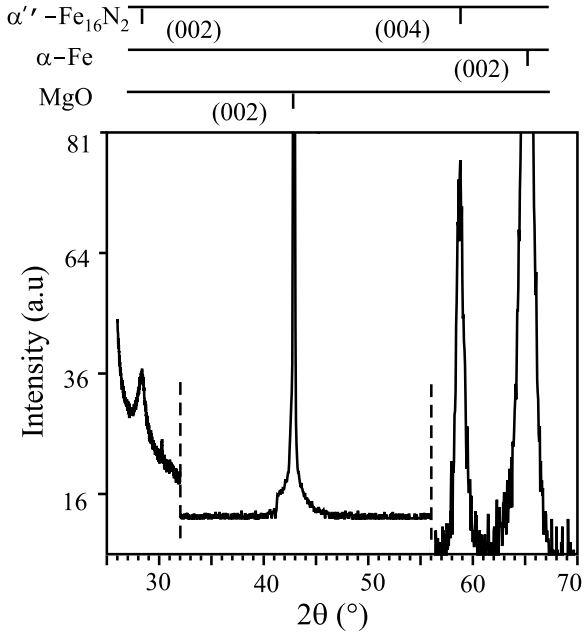

Figure 3.4: *X-ray $\theta-2\theta$ scan for a ∼42 nm thick film containing 22% $\alpha''-Fe_{16}N_2$ grown on a (001) MgO substrate.*

$\alpha''-Fe_{16}N_2$ [44]. The formation of the $\gamma'-Fe_4N$ phase implies that the kinetic barrier for $\gamma'-Fe_4N$ formation can be overcome at 200°C. By decreasing the deposition temperature to 150°C, it was possible to grow a sample containing only a mixture of $\alpha''-Fe_{16}N_2$ and Fe. However, the results could not be reproduced. The films containing $\alpha''-Fe_{16}N_2$ were also investigated with VSM (not shown). For the sample containing 22% $\alpha''-Fe_{16}N_2$, the measured hysteresis loop was square with a coercive field of ∼200 Oe. This value is a factor of 5 higher than the coercive fields measured for epitaxial $\gamma'-Fe_4N$ films grown on (001) MgO substrates of comparable thickness (see chapter 4 for details). The present method might lead to the formation of pure $\alpha''-Fe_{16}N_2$ films if the growth conditions are properly tuned.

3.4 $\gamma'-Fe_4N$, $\varepsilon-Fe_xN$

Contrary to $\alpha''-Fe_{16}N_2$, the $\gamma'-Fe_4N$ phase could be grown by N−assisted MBE. Pure and epitaxial $\gamma'-Fe_4N$ films could be grown on (001) MgO substrates at temperatures from 150°C to 400°C. At a slightly higher deposition temperature (∼460°C), the grown films contained only pure Fe. This suggests that at ∼460°C, decomposition of $\gamma'-Fe_4N$ takes place. $\gamma'-Fe_4N$ could not be grown at room temperature. The films with the best quality (concerning smoothness, crystallinity and purity) were grown at 400°C. Besides elevated temperatures, for the growth of pure $\gamma'-Fe_4N$ films, another crucial parameter was the presence of hydrogen in mixtures with nitrogen in the rf atomic source. There are some possible scenarios to explain the influence of hydrogen, although it's not entirely clear if this parameter has a beneficial effect by itself or in combination with the deposition temperature. Possibly, the hydrogen at the surface is changing the potential landscape for recombination of nitrogen atoms into nitrogen molecules. It cannot be excluded that at 400°C, $\gamma'-Fe_4N$ phase is the most stable phase. This implies that if enough nitrogen is present, this will be the only phase grown (and no $\varepsilon-Fe_xN$ will be formed). The growth and the properties of $\gamma'-Fe_4N$ films are discussed in more detail in chapter 4. Nitride films grown in the presence of high fluxes of nitrogen and temperatures between 150°C and 300°C were grown as mixtures of $\gamma'-Fe_4N$ and magnetic $\varepsilon-Fe_xN$ or as single phase paramagnetic $\varepsilon-Fe_xN$. As shown in the next section, paramagnetic $\varepsilon-Fe_xN$ films could be grown also by post-nitriding epitaxial $\gamma'-Fe_4N$ layers at 300°C.

3.5 $\gamma''-FeN$, $\gamma'''-FeN$

In order to synthesize the $\gamma''-FeN$ and $\gamma'''-FeN$ phases, iron nitride films were grown in two different ways: (I) by molecular beam epitaxy of iron in the presence of nitrogen from the rf atomic source and (II) by post−nitriding

Table 3.2: *Overview of the growth parameters for FeN samples produced by molecular beam epitaxy of iron in the presence of atomic nitrogen.*

Sample	deposition temperature (°C)	growth time (minutes)	thickness (nm)
S1	150	60	18
S2	50	120	36
S3	300	80	18

thin epitaxial $\gamma'-Fe_4N$ films with atomic nitrogen obtained from the same rf atomic source. All the samples were grown with ^{57}Fe. For the samples grown by MBE, the evaporation rate of ^{57}Fe was around 0.027 Å/s, and the atomic source was operated with pure N_2 at a pressure of 1×10^{-1} mbar.

Different FeN samples were grown at three deposition temperatures: 50°C, 150°C and 300°C. An overview of the growth parameters is given in Table 3.2. After growth and cooling to room temperature, the films were capped in−situ with 5 nm of Cu to prevent oxidation. Another way of growing FeN films was by nitriding epitaxially grown $\gamma'-Fe_4N$ films with atomic nitrogen as obtained from the rf atomic source. The $\gamma'-Fe_4N$ films were grown in the same chamber by atomic N−assisted MBE on (001) MgO substrates at a deposition temperature of 400°C. As extensively discussed in chapter 4, the $\gamma'-Fe_4N$ films grown with this method are pure and epitaxial with the $[001]_{\gamma'}//[001]_{\mathrm{MgO}}$ and $(100)_{\gamma'}//(100)_{\mathrm{MgO}}$. The as−grown $\gamma'-Fe_4N$ films were first cooled down to the post−nitriding temperature and subsequently exposed to a flux of nitrogen. In all cases, the rf atomic source was operated with pure N_2 at a pressure of 5×10^{-2} mbar. A number of FeN films were produced by varying the post−nitriding temperature and the post−nitriding time. An overview of the post−nitriding conditions is given in Table 3.3. After post−nitriding, the samples were cooled in−situ to room temperature and subsequently capped with 5 nm of natural Fe or Cu to protect from oxidation.

The stability of the FeN films was probed via annealing experiments per-

Table 3.3: *Growth conditions corresponding to iron nitride samples obtained by post−nitriding epitaxial $\gamma'-Fe_4N$ layers.*

Sample	post−nitriding temperature (°C)	post−nitriding time (h)	thickness (nm)
S4	150	1	15
S5	150	3	15
S6	300	1	15
S7	150	1/2	6

formed in the UHV system at 150°C for 30 minutes. After in−situ cooling, the samples were again measured with CEMS.

Room temperature CEMS spectra measured for FeN samples grown by N−assisted MBE (see Table 3.2) are shown in Fig. 3.5. For these films, the varying parameter was deposition temperature: 150°C for sample S1, 50°C for sample S2 and 300°C for sample S3. The spectra were fitted with Lorentzian−shaped lines and the fit parameters are given in Table 3.4.

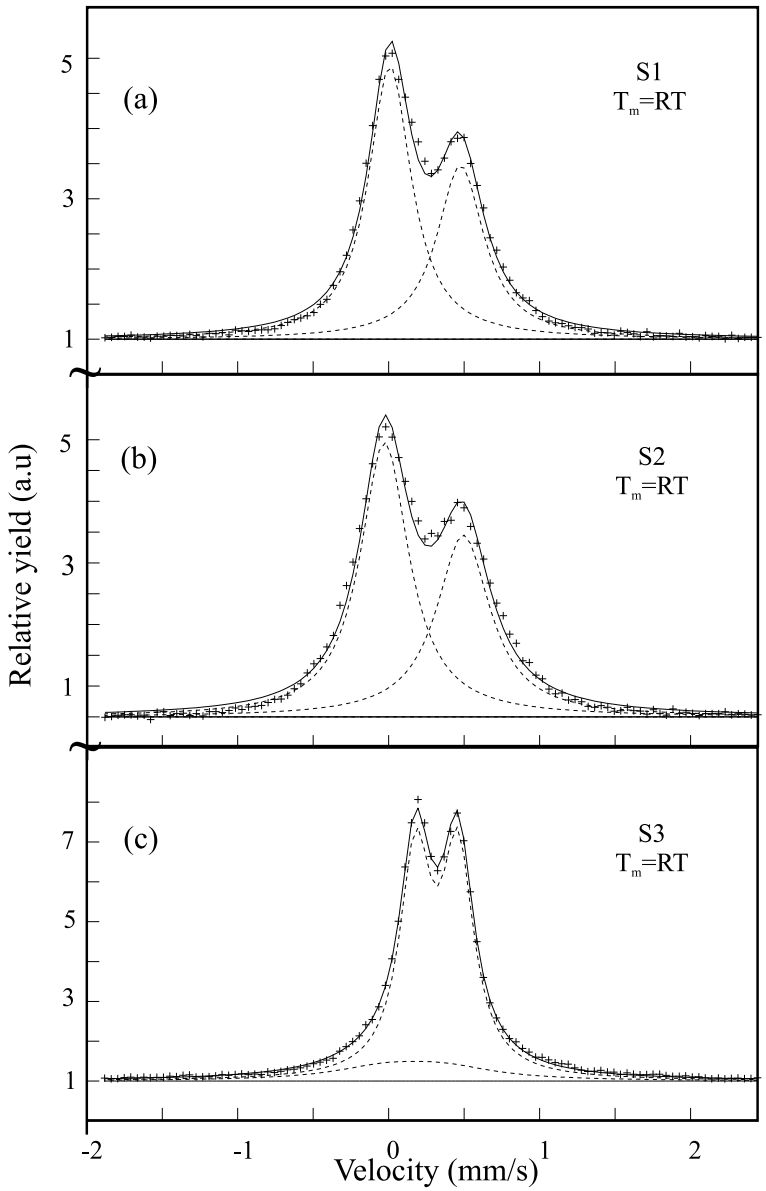

Figure 3.5: *Room temperature CEMS spectra measured for FeN samples grown by N−assisted MBE at three different deposition temperatures: (a) 150°C (sample S1); (b) 50°C (sample S2); (c) 300°C (sample S3).*

Table 3.4: *Fit parameters for FeN samples grown by N−assisted MBE on (001) MgO substrates: δ−isomer shift (all given with respect to α−Fe at room temperature), ε−quadrupole splitting, Γ−linewidth and R.A−relative area.*

Sample	Component	δ(mm/s)	ε(mm/s)	Γ(mm/s)	R.A(%)
S1	$\gamma''-$FeN	0.118	0	0.343	58.78
	$\gamma'''-$FeN	0.583	0	0.379	41.22
S2	$\gamma''-$FeN	0.148	0	0.388	57.73
	$\gamma'''-$FeN	0.602	0	0.431	42.27
S3	$\varepsilon-Fe_{2.108}N$ (FeIII)	0.428	0.280	0.251	84.58
	$\varepsilon-Fe_{2.108}N$ (FeII)	0.280	0.385	0.833	15.42

Before discussing the fit of each spectrum, just by comparing the spectra shown in Fig. 3.5, we can conclude that the films grown at 150°C and 50°C have the same composition (contain the same phase or phases) while the film grown at a much higher deposition temperature, 300°C, is clearly a different phase. During growth, both the growth rate of Fe and pressure of nitrogen in the atomic source were identical for all samples. This corresponds to a constant [Fe/N] arrival rate at the surface. If the uptake rate of nitrogen is independent of temperature, the growth of a different phase at 300°C as compared to 150°C and 50°C suggests a higher stability of this phase. The spectrum in Fig. 3.5 (c) clearly corresponds to a paramagnetic ε phase. The experimental data were fitted with two quadrupole doublets. Based on the ordering model proposed by Jack [22], the $\varepsilon-Fe_xN$ phase could be identified as the $\varepsilon-Fe_{2.108}N$ phase.

On the other hand, the spectra in Fig. 3.5 (a) and (b) can be fitted in two different ways. As shown in Fig. 3.5 (a) and (b), the experimental data can be satisfactorily fitted with the combination of two singlet lines. Based on Mössbauer data previously reported [35, 36, 37, 38], the two singlet lines could be identified as being the signature of the $\gamma''-$FeN phase (the singlet line with the lower isomer shift) and the $\gamma'''-$FeN phase (the singlet line with the higher isomer shift). In both samples, the relative amount of each phase is the same.

Another possibility for fitting the experimental data is shown in Fig. 3.6 (b). Here we show the CEMS spectrum corresponding to sample S1 (grown at 150°C). For comparison reasons we show in Fig. 3.6 (a) the spectrum for the same sample fitted with two singlet lines, already shown in Fig. 3.5 (a). As shown here, an equally satisfactorily fit can be obtained with a singlet line and a quadrupole doublet. The fit parameters for the singlet line coincide with the parameters corresponding to the $\gamma''-$FeN phase. For the quadrupole doublet, the fit parameters are: $\delta\sim0.33$ mm/s and $\varepsilon\sim0.50$ mm/s. Note that all the CEMS spectra fitted with a combination of two singlet lines can be fitted as well with a singlet line and a quadrupole doublet (similar hyperfine parameters). So far, there is no strong experimental evidence for the existence of a

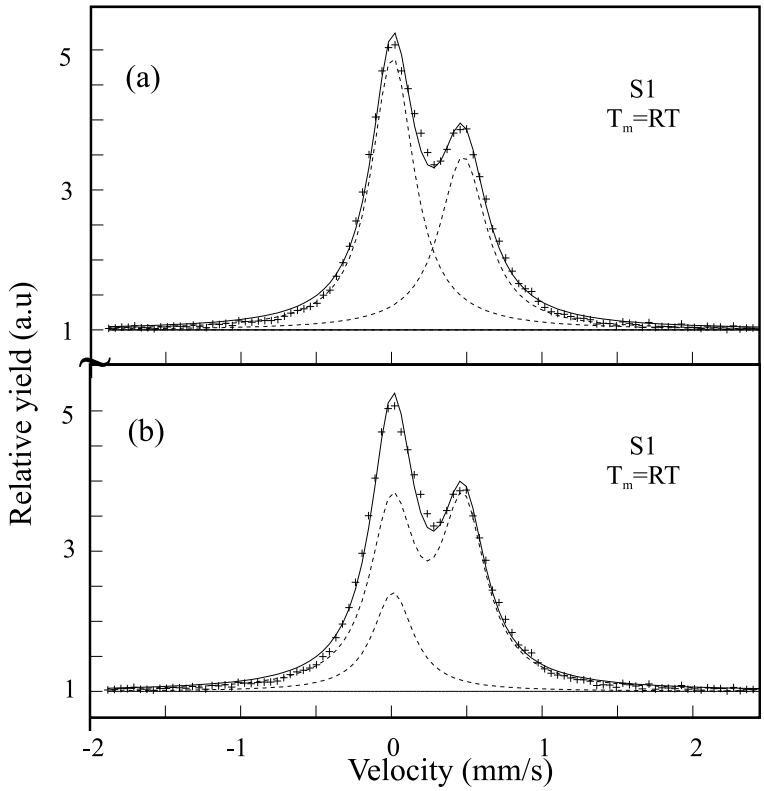

Figure 3.6: *Room temperature CEMS spectra for sample S1 (grown at 150°C) fitted in two different ways: (a) combination of two singlet lines and (b) singlet line and a quadrupole doublet.*

$\gamma'''-$FeN phase. The results from CEMS measurements do not yield straightforward information on the structure. On the other hand, only in the NaCl structure ($\gamma'''-$FeN) the N atoms occupy the octahedral sites, as it is the case for all the other iron nitride phases. For the iron nitrides, there is an increasing trend of the isomer shift with increasing nitrogen content in the phase. For the $\gamma''-$FeN phase, the measured isomer shift of 0.118 mm/s doesn't follow this trend, pointing to a different type of site. Indeed, in the ZnS$-$type structure ($\gamma''-$FeN), the N atoms occupy tetrahedral interstitial sites instead of octahedral (see Fig. 3.2). According to our CEMS investigation, the FeN films grown at 150°C are either a mixture of $\gamma''-$FeN and $\gamma'''-$FeN phases, or $\gamma''-$FeN in a mixture with a second phase which is possibly due to vacancies. The results from both models are in a way contrary to what was reported so far on the growth of these phases by sputtering methods. In all the reported CEMS spectra, besides two singlet lines also a quadrupole doublet of significant relative area was present (usually in a higher fraction than the one corresponding to the $\gamma'''-$FeN). While the two singlet lines were assigned to the $\gamma''-$FeN and $\gamma'''-$FeN phases, the quadrupole doublet (isomer

shift δ=0.32 mm/s and quadrupole splitting ε= 0.77 mm/s) was argued to be due to impurities and defects in the $\gamma'''-$FeN phase (NaCl−type) [38].

As discussed earlier, our CEMS data can be also fitted with a singlet line and a quadrupole doublet. The FeN films studied here were grown in a UHV system. Therefore, we expect no significant amount of impurities (O, C) to be present in the films. Moreover, our doublet has a lower quadrupole splitting ($\varepsilon\sim$0.5 mm/s) than what was reported ($\varepsilon\sim$0.77 mm/s). Consequently, within the model containing the doublet, this should correspond to a different phase. This could appear due to vacancies in either the $\gamma''-$FeN or the $\gamma'''-$FeN phase.

The information obtained from CEMS measurements is not sufficient to make a precise assignment of each component to an iron nitride phase. Accurate stoichiometry and structure analysis could yield the extra information needed. To gain some extra insight into the properties of our films, we performed low temperature CEMS measurements. 90 K CEMS spectra are shown in Fig. 3.7: (a) for a FeN film [sample S2] and (b) for a $\varepsilon-Fe_{2.108}N$ film [sample S3]. The room temperature CEMS spectra corresponding to the two samples were shown in Fig. 3.5 (b) and (c). Comparing the spectra measured at 90 K with the ones at room temperature (see Fig. 3.8), we can conclude that besides the appearance of a broad magnetic component, both spectra retain the shape

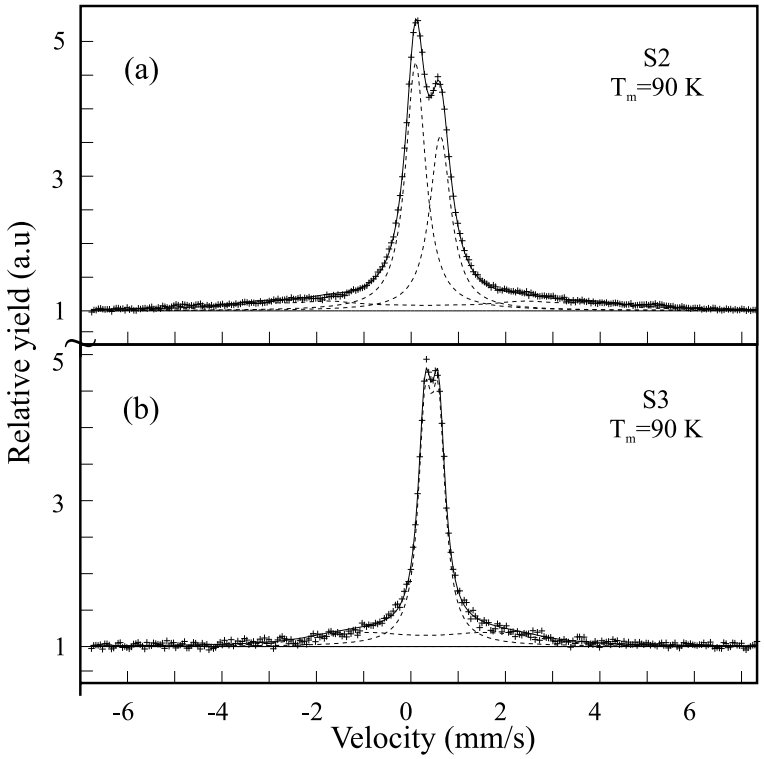

Figure 3.7: *90 K CEMS spectra corresponding to FeN samples grown by N−assisted MBE: (a) sample S2 grown at 50°C and (b) sample S3 grown at 300°C.*

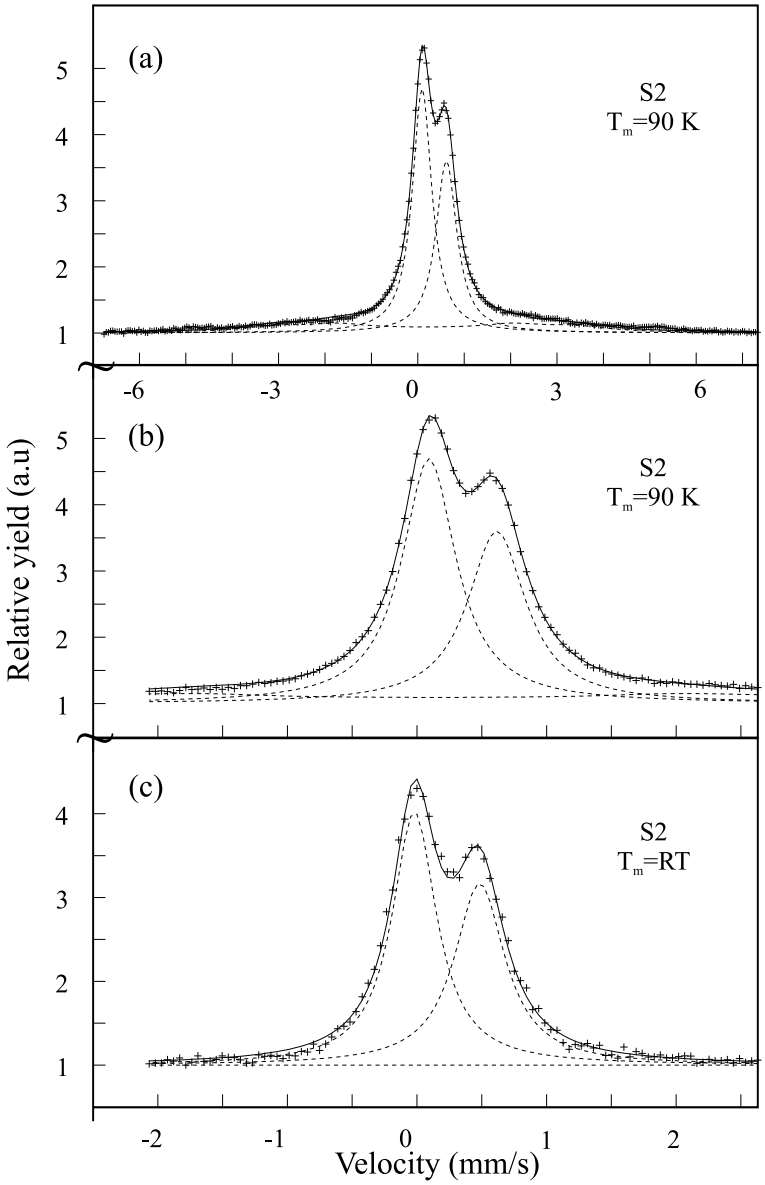

Figure 3.8: *CEMS spectra measured for sample S2 at: (a), (b) both at 90 K and shown on a different velocity scale range, (c) at RT.*

measured at room temperature. This implies that no magnetic transition takes place down to 90 K for these films. The broad magnetic component might originate from the two interfaces (iron nitride−MgO and iron−nitride−Cu). Also, it cannot be excluded that part of this intensity is due to an ε phase also present in the RT CEMS spectra which was not fitted. Like for the RT CEMS spectrum, the main intensity in Fig. 3.8 (a), (b) can be equally satisfactorily fitted with two singlet lines (γ'' and γ''') or a singlet line (γ'') and a doublet. There is no significant difference in the relative fraction of the two phases in

the RT spectrum as compared with the 90 K spectrum.

Room temperature CEMS spectra measured for FeN samples produced by post−nitriding $\gamma'-Fe_4N$ films (see Table 3.3) are shown in Fig. 3.9. For all the

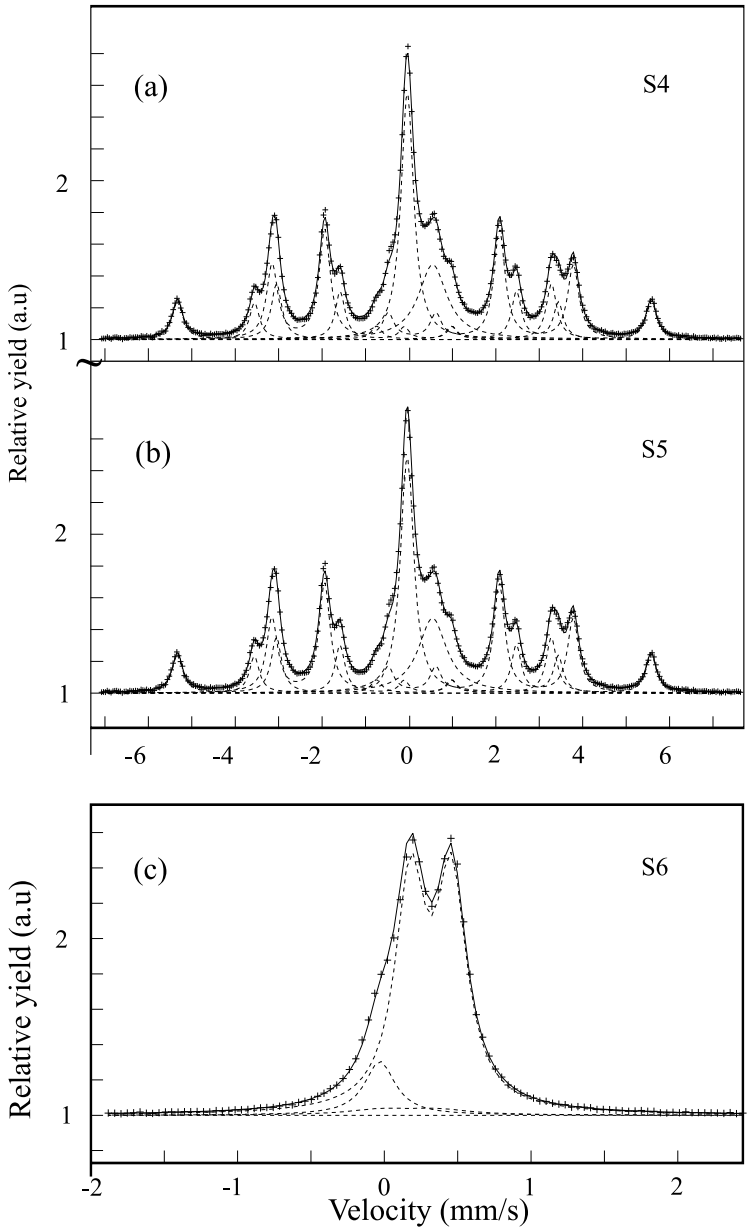

Figure 3.9: *Room temperature CEMS spectra for FeN samples grown by post nitriding of epitaxial $\gamma'-Fe_4N$ thin films: (a) at 150°C for 1 h [sample S4], (b) at 150°C for 3 h [sample S5] and (c) at 300°C for 1 h [Sample S6].*

samples, the thickness of the starting $\gamma'-Fe_4N$ layer was 15 nm. The spectra in Fig. 3.9 (a) and (b) are both fitted with a combination of three magnetic sextets corresponding to the $\gamma'-Fe_4N$ phase and two singlet lines corresponding

to the $\gamma''-$FeN and $\gamma'''-$FeN phases. The Mössbauer parameters of the two singlet lines are close to the ones given in Table 3.4. Similar to the CEMS spectra measured for the FeN samples grown by N−assisted MBE, a fit made with the combination of two singlet lines (γ'' and γ''') can be replaced with a fit made with the combination of a singlet ($\gamma''-$FeN) and a doublet. On the other hand, the spectrum in Fig. 3.9 (c) has a very different appearance. The main intensity in this spectrum coincides with the spectrum shown in Fig. 3.5(c), which we identified as the $\varepsilon-Fe_{2.108}N$ phase. The shoulder on the left side of the spectrum can be well fitted if an extra singlet line is introduced in the fit. This singlet line corresponds to the $\gamma''-$FeN phase.

Independent of the exact stoichiometry of the FeN phase (mixture of γ'' and γ''' or γ'' and a second phase with vacancies) formed upon post−nitriding epitaxial $\gamma'-Fe_4N$ layers, it can be concluded that depending on temperature, there are two behaviors: a low temperature ($\leq$150°C) and a high temperature behavior (at 300°C). At temperatures equal to or below 150°C, the exposure of a $\gamma'-Fe_4N$ film to atomic N results in a partial phase transformation of the iron nitride layer into a FeN phase. The phase transformation from $\gamma'-Fe_4N$ to the FeN phase must take place directly, without the formation of an intermediate ε phase. For a post−nitriding time of 1 h, only 26% of the $\gamma'-Fe_4N$ phase is transformed into the FeN phase. As shown in Fig. 3.9 (b), increasing the post-nitriding time to 3 h, it is still not sufficient to obtain a complete phase transformation of the $\gamma'-Fe_4N$ layer. In this case, the fraction of the FeN phase is 37%. It is very likely that after the formation of an FeN layer of a certain thickness, this acts as a barrier for atomic nitrogen atoms. If the post−nitriding is done at a higher temperature (300°C), the phase transformation of the $\gamma'-Fe_4N$ layer is complete, pointing to a higher diffusion of the N atoms as compared with 150°C. In this case, most of the $\gamma'-Fe_4N$ film is transformed into a $\varepsilon-Fe_{2.108}N$ phase. This film contains without doubt also some $\gamma''-$FeN phase (shoulder on the left of the spectrum). On the other hand, we cannot say for sure if a small fraction of $\gamma'''-$FeN is also present. The contribution of this phase to the CEMS spectrum cannot be separated. This result suggests that the phase transformation from the γ' phase to the ε phase goes via the γ'' and not directly, as reported by Mijiritskii *et al.* [44].

The stability of the FeN phases was studied by annealing a FeN sample grown by post−nitriding. For this experiment the thickness of the $\gamma'-Fe_4N$ layer was of only 6 nm. Such a thin layer was expected to be fully nitrided at 150°C for 30 minutes. After growth and in−situ cooling to room temperature, the film was capped with Cu, and ex−situ measured with CEMS. The annealing step was done in vacuum at 150°C for 30 minutes. After cooling, the sample was again measured with CEMS. The CEMS spectra measured after growth and after the annealing step are shown Fig. 3.10 (a) and (b) respectively. As expected, for the as−grown sample, the measured CEMS spectrum can be very well fitted only with two singlet lines corresponding to the $\gamma''-$FeN (67%)

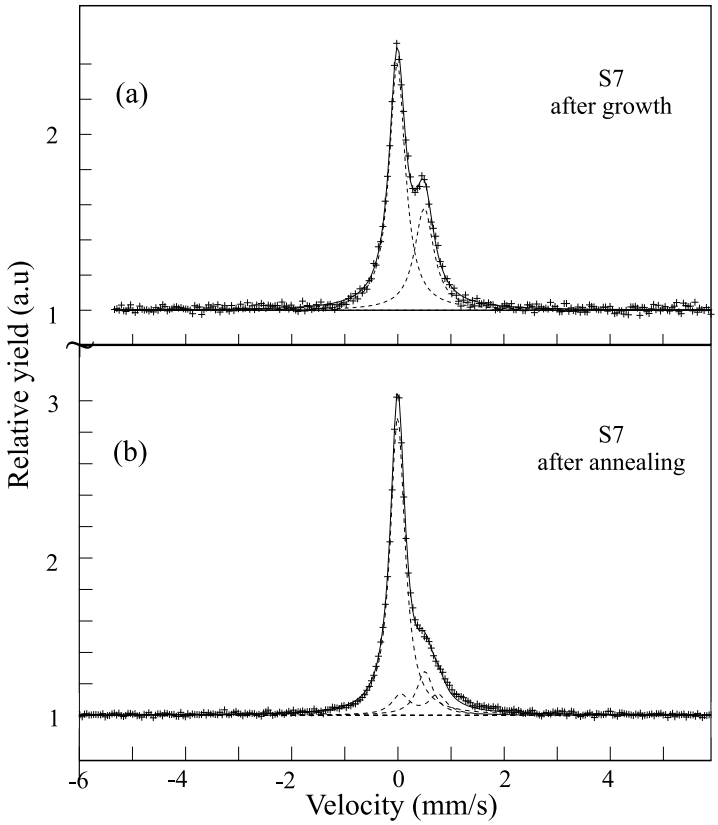

Figure 3.10: *Room temperature CEMS spectra corresponding to an FeN sample obtained by post−nitriding a thin (6 nm) epitaxial $\gamma'-Fe_4N$ film at 150°C for 30 minutes measured: (a) after growth and (b) after annealing at 150°C for 30 minutes.*

and the $\gamma'''-$FeN (33%). This corresponds to a γ''/γ''' relative fractions ratio of 2.03. After the annealing step, there is a clear change in the spectrum. The spectrum is fitted with two singlet lines and an additional doublet. The fraction of the doublet is 12.2% and could be due to the interfaces or/and a paramagnetic ε phase. The ratio of the relative areas of the two singlet lines, $\gamma''-$FeN/$\gamma'''-$FeN is now 6.03. Comparing the two spectra shown in Fig. 3.10, we can conclude that upon annealing, part of $\gamma'''-$FeN transforms into $\gamma''-$FeN. If the as−grown film is a mixture of $\gamma''-$FeN and a second phase containing vacancies, upon annealing, part of the phase containing vacancies could transform to an ε phase. The N set free in this process will occupy vacancies, and therefore, this will result in an increase of the relative fraction of the $\gamma''-$FeN phase.

Additionally, all the samples were characterized ex−situ with XRD. $\theta-2\theta$ scans with 0° or 5° offset were measured. The measured scans are shown in Fig. 3.11 for the FeN films grown by N−assisted MBE and in Fig. 3.12 for the FeN films produced by post−nitriding γ' layers (only the 5° offset scans).

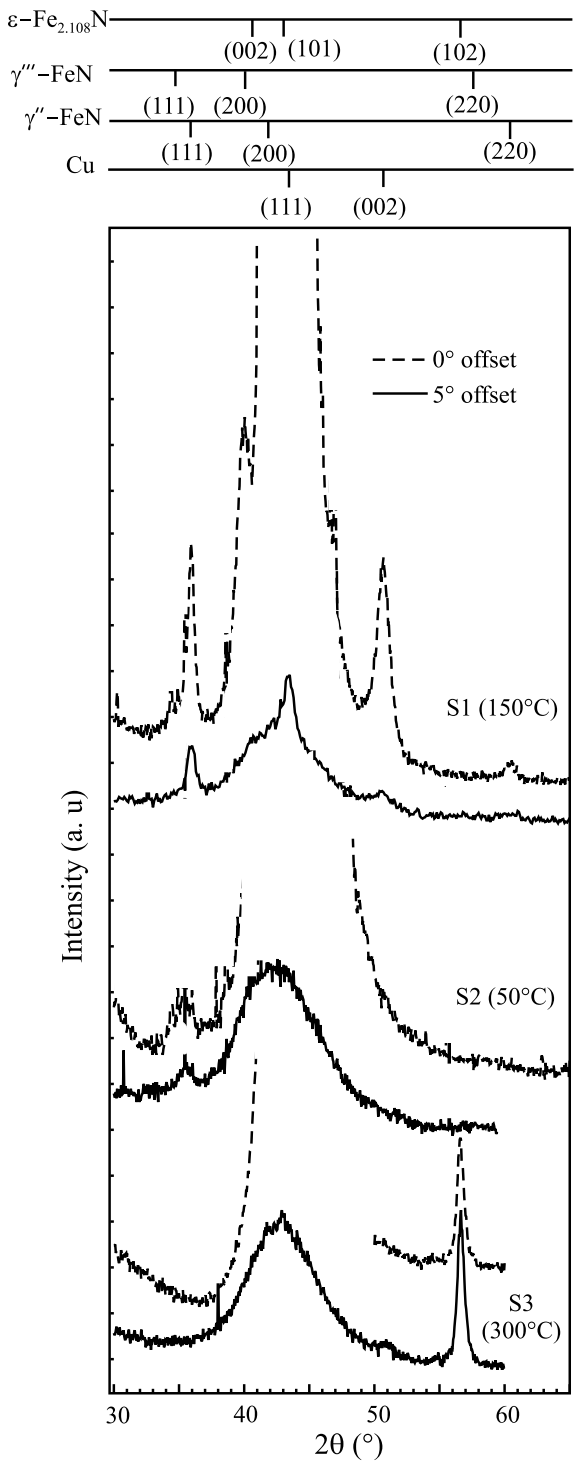

Figure 3.11: *X−ray θ−2θ scans measured for FeN films grown by N−assisted MBE.*

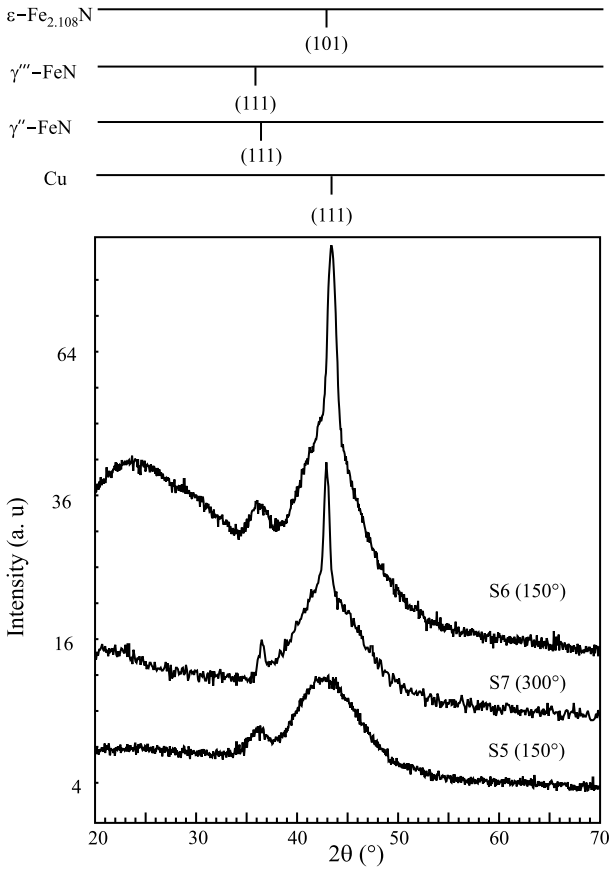

Figure 3.12: *X−ray θ−2θ scans measured for FeN films grown by post−nitriding.*

In all the XRD scans we can identify a peak at $2\theta \sim 36°$. This corresponds to the (111) reflection belonging to a $\gamma''-$FeN phase with a lattice constant $\sim$4.32 Å. This value is in good agreement with what was reported so far. On the other hand, we do not have clear evidence for a second peak which could correspond to the (111) reflection of a phase with a lattice constant $\sim$4.5 Å. This value corresponds to the experimental value reported so far for the $\gamma'''-$FeN phase. It is worth mentioning that for this phase, the lattice parameter predicted theoretically is lower (between 3.9 Å and 4.2 Å). As shown in Fig. 3.11, the (111) reflection peak is quite broad indicating a high degree of disorder. Some improvement of the quality (narrowing of the peak) is seen if the growth temperature is increased (see the scans for S1 and S2 in Fig. 3.11). A similar trend is observed for the samples grown by post−nitriding (see Fig. 3.12). The XRD results point to a polycrystalline FeN phase in all samples. This is in a way a surprising result for the samples grown by post−nitriding epitaxial [001] oriented $\gamma'-Fe_4N$ films.

3.6 Conclusions

N−assisted MBE and/or post−nitriding can be applied successfully to produce most of the existing iron nitride phases. Depending on growth parameters such as deposition temperature, pressure of nitrogen and hydrogen in the rf atomic source, different phases were grown. The metastable character of all iron nitrides makes deposition temperature a key factor in determining which phase is formed. The $\alpha'-Fe_8N$ and $\alpha''-Fe_{16}N_2$ could not be produced by MBE growth of iron in the presence of nitrogen from the rf atomic source. Fractions of $\alpha''-Fe_{16}N_2$ phase were obtained in films grown by post−nitriding epitaxial Fe layers (freshly grown layers) at 200°C. Contrary to $\alpha''-Fe_{16}N_2$, the $\gamma'-Fe_4N$ phase could be grown by N-assisted MBE. This is explained in more detail in chapter 4. At low deposition temperatures (below 150°C) and high pressures of nitrogen, N−assisted MBE growth and post−nitriding of epitaxial $\gamma'-Fe_4N$ layers were applied to probe the growth of nitride phases present at the high−nitrogen content side of the phase diagram ($\gamma''-$FeN and $\gamma'''-$FeN). Quite certainly, the $\gamma''-$FeN phase can be formed. The additional phase present could be the $\gamma'''-$FeN phase, although we do not have strong evidence for this. The extra phase could also correspond to a $\gamma''-$FeN phase containing vacancies. If the same growth parameters (and methods) are used at a higher temperature (300°C), an $\varepsilon-Fe_{2.108}N$ phase is formed. These results suggest that at high temperatures, the phase transformation from γ' to ε is taking place via the γ'' phase, while at lower temperatures (below 150°C), $\gamma'-Fe_4N$ transforms to another fcc phase, the $\gamma''-$FeN phase.